Random singlet phase of cold atoms coupled to a photonic crystal waveguide

David Z. Li,[1] Marco T. Manzoni,[1] and Darrick E. Chang[1,2]
[1]*ICFO-Institut de Ciencies Fotoniques, The Barcelona Institute of Science and Technology, E-08860 Castelldefels (Barcelona), Spain*
[2]*ICREA-Institució Catalana de Recerca i Estudis Avançats, E-08015 Barcleona, Spain*

(Received 5 May 2020; revised 13 May 2021; accepted 29 June 2021; published 26 July 2021)

Systems consisting of cold atoms trapped near photonic crystal waveguides have recently emerged as an exciting platform for quantum atom-light interfaces. Such a system enables realization of tunable long-range interactions between internal states of atoms (spins), mediated by guided photons. Currently, experimental platforms are still limited by low filling fractions, where the atom number is much smaller than the number of sites at which atoms can potentially be trapped. Here, we show that this regime in fact enables interesting many-body quantum phenomena, which are typically associated with short-range disordered systems. As an example, we show how the system can realize the so-called "random singlet phase" (RSP), in which all atoms pair into entangled singlets, but the pairing occurs over a distribution of ranges as opposed to nearest neighbors. We use a renormalization group method to obtain the distribution of spin entanglement in the RSP, and show how this state can be approximately reached via adiabatic evolution from the ground state of a noninteracting Hamiltonian. We also discuss how experimentally this RSP can be observed. We anticipate that this work will accelerate the route toward the exploration of strongly correlated matter in atom-nanophotonics interfaces, by avoiding the requirement of perfectly filled lattices.

DOI: 10.1103/PhysRevA.104.013523

I. INTRODUCTION

In recent years, there has been considerable effort in interfacing atoms with nanophotonic structures [1,2], including nanofibers [3–9] and photonic crystal waveguides (PCWs) [10–14]. The predominant aim initially was to utilize the strong light-matter interactions for applications within quantum information processing [15–19]. More recently, however, it has been realized that these atom-nanophotonics interfaces also open up new paradigms to explore quantum many-body physics [2,20–25].

In particular, when an atomic transition frequency lies in a bandgap of a PCW, a photon emitted from an atom becomes an evanescent wave and forms a bound state around the atom. These bound states, with a tunable evanescent length [20,21,26–29], can facilitate interesting interactions like long-range spin models [22,30], strong spin-motion coupling [23], or long-range interactions between photons [31,32].

These proposals typically require perfect filling of the lattice sites where atoms can potentially be trapped, which is a challenge in current experiments [12,13]. Here, we show that the combination of long-range interactions and low filling enables the realization of novel many-body physics, allowing the system to mimic a spin chain with short-range, random interaction strength [33,34]. In particular, under certain conditions, the ground state of the system becomes a "random singlet phase" (RSP), where all atoms entangle into singlet pairs, but the pairing occurs over a distribution of ranges instead of between nearest neighbors. We analyze the main properties of this phase, and discuss how it can be prepared and observed in a realistic PCW system.

II. THE HAMILTONIAN OF THE SYSTEM

A photonic crystal (PhC) is a periodic dielectric structure that controls the propagation of light. Due to the periodicity, the dispersion relation ω_k versus Bloch wave vector k of guided modes is describable by bands [Fig. 1(b)]. We assume that the atomic optical transition (involving ground state $|g\rangle$ and excited state $|e\rangle$) is situated within a bandgap, a frequency window in which no propagating modes exist. This prevents an excited atom from decaying into $|g\rangle$ by emitting a guided photon; however, the state $|e\rangle$ can become dressed by a photon bound state localized a distance L around the atom [Fig. 1(a)]. Given a second atom in its ground state within a distance $\sim L$ of the first, the pair can exchange their excitations via the bound photon, resulting in an effective spin interaction. In principle, this spin interaction can occur with a high fidelity in spite of atomic spontaneous emission and photon losses, provided that the PhC structure has a large cooperativity (see Appendix A). However, in practice, it would be difficult to directly observe and manipulate the dynamics, given the rapid spontaneous emission rate (and even larger coherent spin interaction rate) associated with the excited state, and furthermore, it would be difficult to tune the interaction rate with time. To fix these issues, it is convenient to introduce an additional metastable state $|s\rangle$, which is coupled to $|e\rangle$ via an external laser field with Rabi frequency $\Omega(t)$ [Fig. 1(a)]. Under certain conditions [20] (also see derivation in Appendix A), the state $|e\rangle$ and its photon bound state are only virtually excited, allowing the dynamics to be projected into the $\{|g\rangle, |s\rangle\}$ manifold with the effective Hamiltonian,

$$\hat{H}_{\rm int}^{N} = \sum_{i<j} \hat{H}_{ij} = (1/2) \sum_{i<j} J_{ij}(t)\left(\hat{\sigma}_x^i \hat{\sigma}_x^j + \hat{\sigma}_y^i \hat{\sigma}_y^j\right), \quad (1)$$

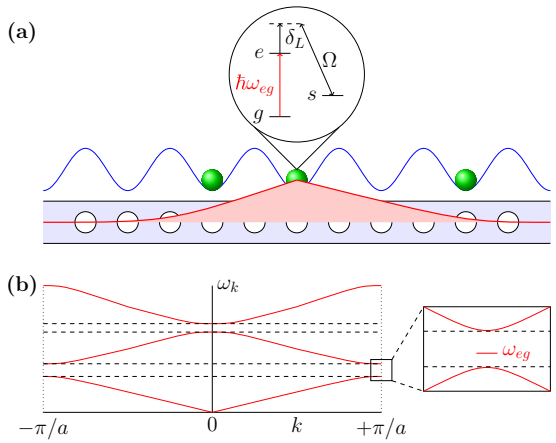

FIG. 1. (a) Schematic illustration of setup, consisting of a sparse and random filling of cold atoms [shaded (green) balls] tightly trapped in a lattice potential [(blue) periodic curve] near a 1D PCW. The atoms have a Λ-level scheme, with the ground (g) to excited (e) state transition frequency being ω_{eg}, and the excited and a metastable state (s) coupled by a Raman laser with Rabi frequency Ω and detuning δ_L. If ω_{eg} lies in the bandgap of the PhC, a photon bound state can form around the atom, illustrated as the (red) decaying envelope. (b) Typical band structure of a 1D PhC with bandgaps, with guided mode frequency ω_k as a function of Bloch wave vector k. The zoom-in rectangle shows the atomic transition frequency ω_{eg} situated in a bandgap and close to a band edge.

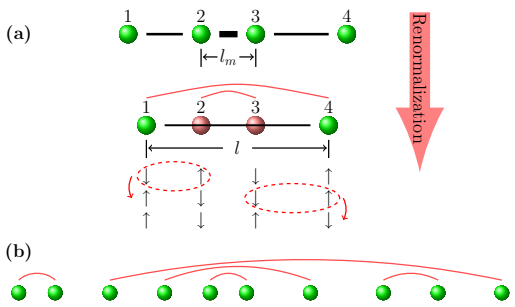

FIG. 2. (a) Illustration of renormalization process and interactions mediated by singlet pairs for the case of four atoms. In the top line, atoms 2 and 3 experience the strongest interaction (thick black line) due to their proximity, so (in the second line) they form a singlet pair [indicated by the (red) line above the atoms] and can be "frozen out" of the 1D chain (indicated by transparent red). Below, we indicate half of the singlet state, with atom 2 initially in state $|\uparrow\rangle$ and atom 3 in state $|\downarrow\rangle$. (First line) If atoms 1 and 4 are in states $|\downarrow\rangle$ and $|\uparrow\rangle$, respectively, atoms 1 and 2 can virtually exchange their spins [dashed (red) circle] at a high energy cost. Atoms 2 and 3 can return to the singlet state (third line) if 3 and 4 virtually exchange their spins as well [second line, dashed (red) circle]. The entire process overall results in an effective interaction between atoms 1 and 4 mediated by the singlet pair of atoms 2 and 3. The effective distance l between atoms 1 and 4 is therefore "renormalized" and shrunk by an amount of d_{eff} (given in the text). This procedure generates pair nesting configurations where singlet pairs sit inside longer ones. (b) A representative ground state of the RSP for 10 atoms.

where $\hat{H}_{ij} = (J_{ij}(t)/2)(\hat{\sigma}_x^i\hat{\sigma}_x^j + \hat{\sigma}_y^i\hat{\sigma}_y^j)$ denotes the spin-flip interaction between atoms i and j ($i, j = 1, ..., N$ and N is the total number of atoms), with $\{|g\rangle, |s\rangle\}$ being treated as pseudospins $\{|\uparrow\rangle, |\downarrow\rangle\}$, and $\{\hat{\sigma}_x, \hat{\sigma}_y\}$ the Pauli matrices. $J_{ij}(t) = J_0(t)\exp(-|x_i - x_j|/L)$ where $J_0(t) \propto \Omega(t)$ is a tunable interaction strength proportional to the external field, and x_i, x_j are the positions of atom i and j. When the atoms are trapped in discrete positions (integer multiples of the lattice constant), but fill only a small fraction of all possible sites, the distances $|x_i - x_j|$ and the interaction strengths J_{ij} become random (over a set of possible discrete values). The dependence of J_0 and L on system parameters (such as laser detunings, band edge curvature, etc.) are described further in [20] and Appendix A, but are not of paramount importance here.

III. A RENORMALIZATION GROUP APPROACH

The salient properties of the ground state can be obtained using the renormalization group (RG) procedure [33,34]. Given a pair of atoms (i and $i+1$) separated by the shortest distance [denoted as $l_m < l$, where l is any other coupling distance in the system; first row in Fig. 2(a)], and thus experiencing the strongest interaction, we first diagonalize the system around $\hat{H}_{i,i+1}$ and treat the rest of Eq. (1) as a perturbation. For positive J_0, the ground state of $\hat{H}_{i,i+1}$ is a singlet: $|S\rangle = (1/\sqrt{2})(|\uparrow\rangle_i|\downarrow\rangle_{i+1} - |\downarrow\rangle_i|\uparrow\rangle_{i+1})$. A spin-flip interaction of one of these atoms (i) with another atom $j \neq i, i+1$ would bring the pair out of the singlet state, at a high energy cost. However, through a second-order process, atom $i+1$ can interact with atom $j' \neq j, i, i+1$, which brings the pair back to the singlet and results in an effective spin-flip interaction between atoms j and j'. Remarkably, the new total effective Hamiltonian H_{int}^{N-2} for the remaining $N-2$ atoms takes exactly the same form as Eq. (1), but where the distance between atoms on *opposite* sides of the already paired atoms (i and $i+1$) is shortened or *renormalized* (Fig. 2): $\tilde{J}_{jj'} \to J_0\exp[-(|x_j - x_{j'}| - d_{\text{eff}})/L]$, where $d_{\text{eff}}/L = 2\,l_m/L + \ln(1 - 2e^{-l_m/L} + 2e^{-2\,l_m/L})$, and the new "effective distance" between atoms j and j' becomes $l \equiv |x_j - x_{j'}| - d_{\text{eff}}$ [second row in Fig. 2(a)] (see Appendix B). One can then repeat this argument, progressively eliminating the next strongest interacting pair with correspondingly larger l_m. The final result is a many-body ground state composed of only singlet pairings, but not necessarily between nearest neighbors [Fig. 2(b)]: the so-called "random singlet phase" [34].

To quantify the salient properties of the RSP, one can consider the probability density $P(l, l_m)$, where $P(l, l_m)\,dl$ characterizes the probability of finding nearest, unpaired atoms with an effective interaction strength between $J_0\exp(-l/L)$ and $J_0\exp(-(l+dl)/L)$, after all pairs interacting with an effective distance of l_m or less have been frozen into singlets. Instead of working with $P(l, l_m)$ directly, it is more convenient to perform a change of variables to $Q(\lambda, l_m) = l_m P(l, l_m)$ with $\lambda = l/l_m - 1$. It can be shown that the elimination process results in the following evolution or RG flow equation for

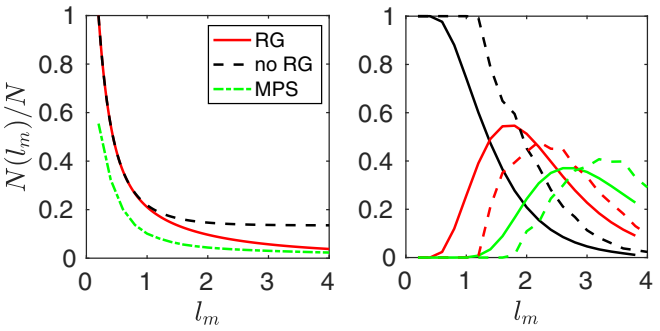

FIG. 3. (Left) Fraction of atoms $N(l_m)/N$ left unpaired, after pairs of atoms with an effective interaction distance up to l_m have been renormalized into singlets. The solid (red) and dash-dotted (green) curves denote the results predicted by the RG flow equations and by numerical MPS simulations, respectively. For comparison, the dashed (black) curve denotes the unpaired atoms without RG, i.e., without allowing nested pairs to occur. (Right) Among the paired atoms, we plot the fractions of nested pairs at l_m. The solid and dashed lines are for RG and MPS simulated results, respectively. The black, dark gray (red), and light gray (green) correspond to nesting orders $n_{l_m} = 0, 1, 2$, respectively. Plotting parameters are $L = 5a$ and 30% filling.

$Q(\lambda, l_m)$ (Appendix C):

$$-Q(\lambda, l_m) + l_m \frac{\partial Q}{\partial l_m} - (1+\lambda)\frac{\partial Q}{\partial \lambda} = Q(0, l_m) \int_0^{\lambda + g(l_m)} d\lambda_1 Q(\lambda_1, l_m) Q(\lambda + g(l_m) - \lambda_1, l_m), \tag{2}$$

where $l_m g(l_m) = \ln[1 - 2e^{-l_m}(1 - e^{-l_m})]$ (both l and l_m have been rescaled by L). We solve Eq. (2) numerically, and in Fig. 3 (left) show the result for the fraction of unpaired atoms as a function of l_m obtained from $Q(\lambda, l_m)$ (Appendix C). As expected, as the cutoff length l_m increases, all atoms become paired. For small N in a given spatial configuration, we can also find the ground state numerically by matrix product state (MPS) algorithms [35]. Given the MPS ground state, we calculate the projection into the singlet state $\langle S|\hat{\rho}_{ij}|S\rangle$ of the two-atom reduced density matrix $\hat{\rho}_{ij}$ of atoms i, j, and identify pairing if the projection is the largest compared to any other combinations ($i, j' \neq j$ or $i' \neq i, j$). Once all pairings are identified for a given configuration [e.g., in Fig. 2(b)], we assume that such a state was formed according to the RG rules and use the expression of $\tilde{J}_{jj'}$ to assign an effective l_m to each pair. In Fig. 3 (left) we plot the MPS result for 10^5 random distributions for $N = 30$. It agrees well with the RG flow equation. The discrepancy for small l_m is attributable mostly to the fact that in the physical system and in the MPS simulations, there is a discreteness of atomic positions, which must, however, be approximated by a smooth distribution to solve Eq. (2) (Appendix C).

To appreciate the importance of interactions mediated by singlet pairs that have been integrated out, we consider the pair nesting structure: the likelihood of finding a singlet pair with n_l other pairs nested inside [e.g., in Fig. 2(a) $n_l = 1$ for pair 1-4, as pair 2-3 is nested inside]. We introduce the *joint distribution*: $P(n_l, l, l_m)\mathrm{d}l$, which gives the probability of finding a coupling of length l *and* containing n_l *nested* pairs inside, when the shortest coupling length in the system is l_m. An RG flow equation can be obtained in a similar fashion as for Eq. (2) (Appendix C). We solve the equation numerically and obtain the fractions of nested pairs as a function of l_m, and plot them in Fig. 3 (right) together with the result from MPS simulations. When l_m is small most of the pairs are un-nested ($n_{l_m} = 0$), indicating the pairing of consecutive atoms, but as l_m increases the fractions of nested pairs ($n_{l_m} = 1$ and 2) increase and overtake the un-nested pairs. The MPS result qualitatively agrees with that of RG. The noticeable shift can be attributed both to the discreteness of atomic positions, and to the relatively small size of the system (30 atoms) used in the simulations, as this is unfavorable to forming long-distance nested pairs.

To qualitatively understand the significant effect of pair renormalization, we also compare the RG result with simply identifying shortest distances between any two neighboring atoms and pairing them up, without any distance renormalization or pair nesting. This pair length distribution can be obtained from $P(0, l_m, l_m)$. In Fig. 3 (left) we plot the number of unpaired atoms in this "no RG" case. One observes that $\sim$15% of atoms remain unpaired as $l_m \to \infty$ [Fig. 3 (right)].

IV. PREPARATION OF THE GROUND STATE IN RSP

Thus far, we have described the ground-state properties of Eq. (1). However, as this is an effective Hamiltonian produced by external laser driving, the ground state cannot be reached by thermalization. Thus, we consider adiabatic evolution from the ground state of a noninteracting Hamiltonian $\hat{H}_0$ which can be easily prepared. Specifically, we consider a time evolution process under $\hat{H}(t) = \cos(\omega t)\hat{H}_0 + \sin(\omega t)\hat{H}^N_{\rm int}$; the initial state at $t = 0$ starts with the ground state of $\hat{H}_0$ and the final state one wants to reach at $t = \pi/2\omega$ is the ground state of $\hat{H}^N_{\rm int}$. The *slew rate* ω characterizes how fast the time evolution happens. One needs to choose $\hat{H}_0$ in a way that $\hat{H}(t)$ avoids extra (nearly) conserved quantities which prevent the initial state from evolving into the interacting ground state. We find that a good candidate consists of an effective magnetic field whose orientation rotates in the x-y plane by a fixed angle from site to site: $\hat{H}_0 = \epsilon_0 \sum_i \hat{\sigma}^i_\perp(\phi_i)$, with $\hat{\sigma}^i_\perp(\phi_i) = \cos\phi_i\, \hat{\sigma}^i_x + \sin\phi_i\, \hat{\sigma}^i_y$ and $\phi_i = (x_i/a)\,\phi_0$, where ϕ_0 is a constant between 0 and 2π. The corresponding initial state of atom i is then given by $(1/\sqrt{2})(|\uparrow\rangle - e^{i\phi_i}|\downarrow\rangle)$.

In practice, the optimal ω will be dictated by a balance of evolving slowly enough to preserve adiabaticity, and fast enough to avoid realistic errors not captured by $\hat{H}^N_{\rm int}$, which in this case consist of the spontaneous emission of atoms and loss of the PhC. The errors associated with nonadiabacity cause the final state to end up in an excited state of $\hat{H}^N_{\rm int}$. Although the scaling of these errors vs ω is generally complicated for a many-body system [36], here we can develop a simple picture based on the observation that the ground state consists of singlet pairs. The Landau-Zener theorem [37–39] implies a singlet will form if the renormalized interaction strength between two atoms exceeds the slew rate ($\tilde{J}_{ij} \gtrsim \omega$).

In order to have a large proportion of long pairs, we choose a relatively low filling fraction and numerically simulate the

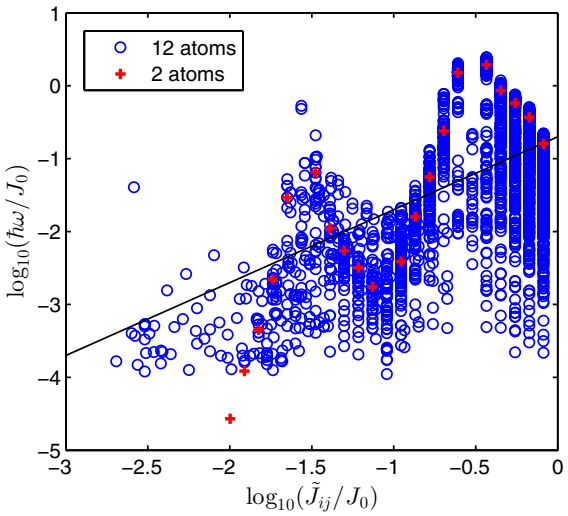

FIG. 4. Slew rate at pair breaking vs binding energy for 1000 random distributions of 12 atoms on 100 trapping sites. For comparison, the result for two atoms is also shown. The relevant parameters are $\epsilon_0 = J_0$, $L = 5\,a$, and $\phi_0 = \pi/6$. The black line is a guide to the eye, showing a $\omega \propto \tilde{J}_{ij}$ scaling.

time evolution of 12 atoms randomly distributed among 100 lattice sites under $\hat{H}(t)$. For each distribution of 12 atoms among 100 lattice sites, we simulate the time evolution by starting from the ground state of $\hat{H}_0$ as the initial state $\psi(t = 0)$, and evolving it to the final state $\psi(t = \pi/2\omega)$ under the time-dependent $\hat{H}(t)$ at a chosen slew rate ω. At the end of the time evolution, we compare the final state with the true ground state of $H^N_{\rm int}$, obtained by direct diagonalization, and see if singlet pairs are broken. We identify the singlet pairs by looking at the singlet fraction in two-atom reduced density matrices. For each distribution, we always begin with a small ω such that the final state will have a high overlap with the true ground state of $H^N_{\rm int}$ (e.g., 99%), where all atoms form into singlet pairs. We then repeat the time evolution at increasingly larger ω, consequently seeing more singlet pairs broken (defined as the singlet fraction dropping below 50%), until there are no singlet pairs left in the final state. In this process, whenever a new singlet pair starts to break, we record the value of ω with the effective interaction strength $\tilde{J}_{ij}$ of the pair. We repeat this procedure for 1000 random distributions, and plot the result in Fig. 4. The values of $\tilde{J}_{ij}$ are ascribed to pairs in a procedure identical to that used in the MPS numerics in Fig. 3. As a guide to the eye, we also plot the scaling $\omega \propto \tilde{J}_{ij}$, as would be expected from the simple Landau-Zener argument.

The full numerics appears consistent with this argument, albeit with a large spread and some oscillatory behavior. The oscillation is an effect that arises even in the problem of $N = 2$ atoms, as the specific distance of separation gives rise to a different effective field direction and $\hat{H}_0$. To confirm this, in Fig. 4 we also plot the result for $N = 2$ atoms. The additional large variation seen for $N = 12$ atoms arises from the combination of many-body effects and sampling over many random configurations. This inevitably results in certain configurations (e.g., three atoms occupying consecutive sites) where RG cannot quantitatively capture the full physics.

With the scaling relation of ω-$\tilde{J}_{ij}$, we next take into account the errors in realistic experiments due to photon loss of the PCW and atomic spontaneous emission, and find the optimal slew rate that will preserve the most singlet pairs at the end of the time evolution. In Appendix A, we present the master equation for the atoms, including the undesired dissipative effects. If the PCW parameters are optimized, one finds an incoherent spin-flip rate of $\sim J_0/\sqrt{C}$. Here, C is the single-atom cooperativity in the PCW, which only depends on the mode volume of the bound state mediating the interaction, and the photon dissipation rate. Since the total evolution time is $T = \pi/2\omega$, the probability that a singlet is lost incoherently is then $P_{\rm inc}(\omega) = J_0\,T/\sqrt{C}$. Without accounting for this incoherent loss, the errors would be purely due to nonadiabacity, and the fraction of *unpaired* atoms at the end of the time evolution due to finite slew rate $F_{\rm unpaired}(\omega)$ can be found by using the scaling between ω and $\tilde{J}_{ij}$ and the relation between the effective coupling length l_m and the fraction of unpaired atoms [e.g., as plotted in Fig. 3 (left)]. Then taking into account incoherent losses, the fraction of *paired* atoms at the end of the time evolution can be obtained as $F_{\rm paired}(\omega) = (1 - F_{\rm unpaired}(\omega))(1 - P_{\rm inc}(\omega))$. Taking a PCW cooperativity of $C = 10^4$ [20] in $P_{\rm inc}$, and optimizing over ω for maximum $F_{\rm paired}(\omega)$, we estimate that $F_{\rm paired}(\omega) \approx 70\%$ for 12% filling fraction. In Appendix D, we also give an analysis of the pair nesting structure at the end of the time evolution when the slew rate is optimized at 12% filling.

V. EXPERIMENTAL DETECTION OF RSP

We envision at least two experimental scenarios in which the RSP could be realized. The first involves atoms that are deterministically trapped at well-controlled positions, with single-atom measurement capabilities. Such a situation could be realized by integrating a tweezer array [40–44] with PCWs [45,46], or with superconducting qubits coupled to microwave PCWs [47]. In that case, the spin correlations associated with the RSP could be directly mapped out. In the second case, neutral cold atoms could be coupled to PCWs in a setup similar to Ref. [13], where the atomic positions are unknown from shot-to-shot, and only global measurements are possible. Then there is no clear way to measure the microscopic properties of entanglement (e.g., nesting), however, one can measure global spin properties instead. A distinguishing characteristic of the ideal RSP is that, being composed globally of singlets, the state has no collective spin angular momentum. Thus measurements of $\hat{S}_\alpha = (\hbar/2)\sum_i \hat{\sigma}^i_\alpha$, $\alpha = x, y, z$ would ideally exhibit zero mean and variance $\langle \hat{S}_\alpha \rangle = \langle \Delta \hat{S}_\alpha \rangle = 0$. An interesting feature of our proposed PCW implementation is that these collective spin properties can be mapped onto and measured in the correlation functions of the outgoing guided light, in a manner similar to the detection of spin squeezing in ensembles [48–50].

VI. CONCLUSIONS

We have shown that the combination of long-range interactions and low filling fraction in atom-PhC interfaces can give rise to novel many-body phases typically associated with short-range, disordered systems, specifically a random

singlet phase. Although the RSP is common to both nearest-neighbor disordered spin systems and atom-PCW interfaces, the longer range interaction and tunability of the latter could more broadly lead to rich physics that is not present in the former case. For example, by tuning the interaction range toward $L \to \infty$, the ground state would eventually become the highly degenerate subspace where the global spin $\vec{S} = 0$, and it could be interesting to explore such a transition. Furthermore, while the nearest-neighbor model is noninteracting (mappable to free fermions by the Jordan-Wigner transformation), our model with extended range is intrinsically interacting. This could allow for the emergence of interesting dynamical effects, such as many-body localization [51,52].

ACKNOWLEDGMENTS

The authors acknowledge funding from the European Research Council (ERC) under the European Union's Horizon 2020 research and innovation programme (Grant Agreement No. 639643, project FOQAL), the Government of Spain (Europa Excelencia Program No. EUR2020-112155, Severo Ochoa Program No. CEX2019-000910-S, and MICINN Plan Nacional Grant No. PGC2018-096844-B-I00), Generalitat de Catalunya through the CERCA programme, Fundació Privada Cellex, Fundació Mir-Puig, and QuantumCAT (Grant No. 001-P-001644, funded through the framework of the ERDF Operational Program of Catalunya).

APPENDIX A: FULL DYNAMICS OF THE SYSTEM WITH DISSIPATION

In this Appendix, we present the full master equation of the atoms coupled to a PCW, and discuss in detail the different dissipation mechanisms.

1. Dissipation without Raman coupling between states $|e\rangle$ and $|s\rangle$

We first consider the case of many two-level atoms with states $|g\rangle$ and $|e\rangle$ trapped near a PCW. In the interaction picture, the interaction between the atom and PCW modes is

$$H_I = \hbar \sum_j \int dk g_k \sigma_{eg}^j \hat{a}_k u_k(z_j) e^{i(\delta_k t + k z_j)} + \text{H.c.}, \tag{A1}$$

where g_k is the coupling strength [20], $\hat{a}_k$ and u_k are the annihilation operator and Bloch function of the PCW modes, respectively, z_j denotes the position of the jth atom, and $\delta_k = \omega_a - \omega_k$ where ω_a is the atomic transition frequency.

In the presence of loss, we can describe the evolution of the system by the master equation $\dot{\rho} = \mathcal{L}_I(t)\rho + \mathcal{L}_\gamma(t)\rho + \mathcal{L}_\kappa(t)\rho$. Here $\mathcal{L}_I(t)\rho = -i/\hbar[H_I, \rho]$ describes the coherent evolution, while the loss mechanisms resulting from spontaneous emission from the atomic excited state (rate γ) and loss of photons in the PCW (rate κ) are described by

$$\mathcal{L}_\gamma \rho = -\frac{\gamma}{2} \sum_j \left(\{\sigma_{ee}^j, \rho\} - 2\sigma_{ge}^j \rho \, \sigma_{eg}^j \right), \tag{A2}$$

and

$$\mathcal{L}_\kappa \rho = -\frac{\kappa}{2} \int dk \left(\{\hat{a}_k^\dagger \hat{a}_k, \rho\} - 2\hat{a}_k \rho \, \hat{a}_k^\dagger \right). \tag{A3}$$

We now consider the case where the atomic transition frequency is near a photonic band edge (frequency ω_b and wave vector k_0), but within the bandgap. We approximate the dispersion relation of the band to be quadratic: $\omega_k \approx \omega_b [1 - \alpha(k - k_0)^2/k_0^2]$, where α characterizes the band curvature, and we define $\Delta = \omega_a - \omega_b > 0$ as the atomic detuning from the band edge. In the limit of $\Delta \to \infty$, the atom and the photons become decoupled. On the other hand, one can perform an expansion in $1/\Delta$, to derive an effective master equation for the atoms alone, due to virtual excitations of the photons. Such an expansion is valid in the limit that $\Delta \gg \kappa, g_c$, where g_c is a coherent coupling strength between the atom and the emergent photon bound state (defined shortly below). Formally, this expansion and elimination of the photon modes can be carried out using the Nakajima-Zwanzig approach in the Born-Markov approximation [53], after which one obtains the following master equation for the reduced density matrix operator, $\rho_s = \text{Tr}_k(\rho)$,

$$\dot{\rho}_s = -\frac{i}{\hbar}[H_I^{\text{eff}}, \rho_s] + \mathcal{L}_\gamma \rho_s + \mathcal{L}_\kappa^{\text{eff}} \rho_s. \tag{A4}$$

To leading order the interaction is described by the effective Hamiltonian,

$$H_I^{\text{eff}} = \frac{g_c^2}{2\Delta} \sum_{j,l} u_{k_0}(z_j) u_{k_0}^*(z_l) \exp[-|z_j - z_l|/L] \sigma_{eg}^j \sigma_{ge}^l, \tag{A5}$$

in which $L = \sqrt{\alpha \, \omega_b/\Delta \, k_0^2}$, and $g_c = g_k \sqrt{2\pi/L}$. The photon loss in the PCW enters at order $\sim 1/\Delta^2$ (corresponding to the amount of photon population generated by an excited atom), and is described by

$$\mathcal{L}_\kappa^{\text{eff}} \rho_s = -\frac{g_c^2 \kappa}{8\Delta^2} \sum_{j,l} u_{k_0}(z_j) u_{k_0}^*(z_l) \left(\{\sigma_{eg}^j \sigma_{ge}^l, \rho_s\} - 2\sigma_{ge}^j \rho_s \, \sigma_{eg}^l \right). \tag{A6}$$

The effect of losses can be revealed by studying the exchange of an excitation between two atoms separated by $|z_1 - z_2| \lesssim L$. From Eq. (A5), the time for exchange is given by $\tau \sim \pi \Delta / g_c^2$, while the total loss is given by $\tau(\gamma \cos^2\theta + \kappa \sin^2\theta)$, where θ is the mixing angle of excitations between being photonic and atomic, and dependent on Δ. Optimizing Δ, we find an exchange error of $\pi/\sqrt{C}$, where $C = g_c^2/\gamma\kappa$ is the single-atom cooperativity.

2. Dissipation with Raman coupling between states $|e\rangle$ and $|s\rangle$

We now examine the case with more complicated internal level structures as depicted in Fig. 1 in the main text. We assume the transition not coupled to the PCW $|s\rangle$-$|e\rangle$ is weakly excited by an orthogonally polarized laser with detuning δ_L and Rabi frequency Ω. We take $\delta_L \gg \gamma$ in which case the atoms are weakly driven and the Raman scattered fields are predominantly centered around the two-photon resonance frequency. In this regime, similar as above, we can obtain effective dynamics for the long-lived atomic ground states $|s\rangle$ and $|g\rangle$. Again using the Nakajima-Zwanzig technique, we obtain H_I^{eff} and $\mathcal{L}_\kappa^{\text{eff}}\rho$ similar to those in Eqs. (A5) and (A6), except that $|e\rangle$ is

replaced by $|s\rangle$, and the strength of the interaction and the loss are renormalized by

$$\frac{g_c^2}{2\Delta} \longrightarrow \frac{g_c^2}{2\Delta_L}\frac{|\Omega|^2}{\delta_L^2} \quad \text{and} \quad \frac{g_c^2\kappa}{8\Delta^2} \longrightarrow \frac{g_c^2\kappa}{8\Delta_L^2}\frac{|\Omega|^2}{\delta_L^2}, \tag{A7}$$

respectively. Here $\Delta_L = \delta_L + \omega_a - \omega_b$, and we make the replacement $\Delta \to \Delta_L$ in the expression for L. The loss of coherence in the ground-state manifold resulting from spontaneous emission into free space is described by

$$\mathcal{L}_\gamma^{\text{eff}}\rho = -\frac{\gamma}{2}\frac{|\Omega|^2}{\delta_L^2}\sum_j \left(\{\sigma_{ss}^j, \rho\} - \sigma_{ss}^j\rho\sigma_{ss}^j - \sigma_{gs}^j\rho\sigma_{sg}^j\right), \tag{A8}$$

where the linewidth of the transition is also renormalized by $|\Omega|^2/\delta_L^2$. Therefore the interaction and losses are all reduced by the same factor. As a result, a spin exchange interaction involving the states $|g\rangle$ and $|s\rangle$ also has an error of $\pi/\sqrt{C}$.

APPENDIX B: DERIVATION OF THE RENORMALIZED HAMILTONIAN

Here, starting from the system Hamiltonian of Eq. (1) in the main text, we derive the effective Hamiltonian that results from integrating out the strongest interacting pair of atoms, which then gives the effective interaction $\tilde{J}_{jj'}$ in the main text.

Let's denote the indices of the spins with the strongest coupling as 1 and 2, and $j \neq 1, 2$ denote all other spins. The full Hilbert space spanned by all the spins can be divided into a low-energy subspace spanned by $|S_{12}\rangle \otimes \{|\sigma_j\rangle, j \neq 1, 2\}$, where $|S_{12}\rangle$ is the singlet state of spins 1 and 2, and $\sigma_j = \uparrow$ or $\downarrow$, and a high-energy subspace spanned by $|T_{12}^{0,\pm1}\rangle \otimes \{|\sigma_j\rangle, j \neq 1, 2\}$, where $|T_{12}^{0,\pm1}\rangle$ is the triplet manifold with the magnetic quantum number of each state denoted explicitly. Accordingly, the full Hamiltonian of the system can be split up into the form,

$$\hat{H}_{\text{int}}^N = \hat{H}_{12} + \sum_{\substack{i=1,2\\ j\neq 1,2}} \hat{H}_{ij} + \sum_{j<j'\neq 1,2} \hat{H}_{jj'}, \tag{B1}$$

where $\hat{H}_{ij} = (J_{ij}/2)(\hat{\sigma}_x^i\hat{\sigma}_x^j + \hat{\sigma}_y^i\hat{\sigma}_y^j)$. The second term on the right-hand side of Eq. (B1) describes the interactions between atoms 1 and 2 with all the other atoms, while the third term describes the interactions between all the atoms excluding 1 and 2. For notational convenience, we will define these second and third terms as $\hat{V}_{\text{od}} = \sum_{i=1,2\, j\neq 1,2} \hat{H}_{ij}$ and $\hat{V}_{\text{d}} = \sum_{j<j'\neq 1,2} \hat{H}_{jj'}$. Our goal is to integrate out atoms 1 and 2, but accounting for the lowest-order nontrivial process. In particular, we consider a quantum fluctuation where one atom $j \neq 1, 2$ interacts with the pair 1,2 via $\hat{V}_{\text{od}}$ and momentarily brings this pair out of the low-energy singlet state $|S_{12}\rangle$, while another atom $j' \neq 1, 2$ also interacts with the pair via $\hat{V}_{\text{od}}$ and brings it back to the singlet state, and thus yielding an effective interaction between atoms j, j'. This is formally encoded in the "Schrieffer-Wolff" transformation [54], given by

$$\hat{H}_{\text{int}}^N \approx -J_{12} + \tfrac{1}{2}\hat{P}_0\left[\hat{S}, \hat{V}_{\text{od}}\right]\hat{P}_0 + \hat{V}_{\text{d}}, \tag{B2}$$

where $\hat{P}_0 = |S_{12}\rangle\langle S_{12}| \otimes \hat{\mathbb{I}}$ projects the pair 1,2 into its low-energy subspace ($\hat{\mathbb{I}}$ is the identity operator acting on the remaining atoms), and $\hat{S} = \sum_{p,q} \frac{\langle p|\hat{V}_{\text{od}}|q\rangle}{E_p - E_q}|p\rangle\langle q|$ with p and q denoting states where the pair 1,2 belong to different subspaces. For example, if $|p\rangle$ is a state in the subspace $|S_{12}\rangle \otimes \mathcal{H}$ (with $\mathcal{H}$ denoting the Hilbert space of remaining spins besides 1,2), with $E_p = \langle S_{12}|\hat{H}_{12}|S_{12}\rangle$, then $|q\rangle$ is a state in the subspace $|T_{12}^{0,\pm1}\rangle \otimes \mathcal{H}$, with $E_q = \langle T_{12}^{0,\pm1}|\hat{H}_{12}|T_{12}^{0,\pm1}\rangle$, or vice versa. The term $\sim\hat{P}_0[\hat{S}, \hat{V}_{\text{od}}]\hat{P}_0$ precisely encodes the effect of quantum fluctuations described above. After some algebra, we reach

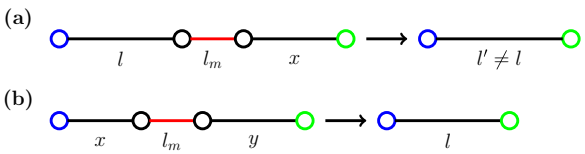

FIG. 5. Illustration of various terms in Eq. (C1). The atoms involved in the RG are denoted by circles. The strongest interacting pair, separated by effective distance l_m (red online), is integrated out, leading to new effective distances between the remaining pair of atoms.

$$\hat{H}_{\text{int}}^N = -J_{12} - \sum_{j\neq 1,2} \frac{(J_{2j} - J_{1j})^2}{2J_{12}} + \hat{V}_{\text{d}}', \tag{B3}$$

with $\hat{V}_{\text{d}}'$ takes the same form as $\hat{V}_{\text{d}}$, but where the bare coupling strength $J_{jj'}$ is replaced by the renormalized value $\tilde{J}_{jj'} = J_{jj'} - \frac{(J_{2j}-J_{1j})(J_{2j'}-J_{1j'})}{J_{12}}$. Plugging in the expression $J_{ij} = J_0\exp(-|x_i - x_j|/L)$, one can show that when atom j and j' sit on the *same* side of atoms 1 and 2, $\tilde{J}_{jj'} \approx J_{jj'}$, whereas when they sit on *opposite* sides of atoms 1 and 2, $\tilde{J}_{jj'} = J_0\exp(-\frac{|x_j - x_{j'}| - d_{\text{eff}}}{L})$, with the expression of d_{eff} given in the main text. Thus, after the two spins with the strongest coupling in the system form into a singlet pair, the form of interactions between remaining spins sitting on opposite sides of spins 1 and 2 stays the same, except their distances are renormalized and shrunk by an amount of d_{eff}. We note in contrast to the nearest-neighbor interactions discussed by [33,34], where only the two atoms nearest the pair see a renormalized interaction, here the interaction of all atoms on opposite sides of the singlet pair becomes stronger due to the mediating effect of the pair.

APPENDIX C: RENORMALIZATION GROUP FLOW EQUATIONS

1. Derivation of the flow equation for the coupling length distribution

Here, we describe further the derivation of the renormalization group Eq. (2) of the main text, and discuss its solution. During the RG process, after all pairs of interacting atoms separated by an effective distance of l_m have been integrated out, the remaining distances l follow a probability distribution $P(l, l_m)\text{d}l$ (normalized so that $\int_{l_m}^\infty dl\, P(l, l_m) = 1$). We next consider how $P(l, l_m)$ evolves when pairs of atoms with effective distances within an infinitesimal range $[l_m, l_m + \Delta]$ are renormalized and effectively removed. There are two processes by which the effective distance l can change (thus modifying the probability distribution). In the first, a pair of atoms [connected by l in Fig. 5(a), blue and black online)

has an effective distance l of interaction, but one of these atoms (right, black) also forms a pair with another atom of effective distance l_m, which is to be renormalized. Once the pair associated with l_m is renormalized (removed), the remaining atom (left, blue) sees an interaction strength with a new effective distance $l' \neq l$ with the atom on the other side of the renormalized pair (right one connected by x or l', green). This reduces the probability of finding the effective distance l in the chain. Thus the probability change caused by this process needs to be subtracted from $P(l, l_m)$, which gives the second term in the larger square bracket on the right-hand side (RHS) of Eq. (C1) below. In the second process, two adjacent pairs of atoms with effective distances x [connected by x in Fig. 5(b), blue and black) and y [connected by y in Fig. 5(b), black and green] are connected by an effective distance l_m. Once the pair of (black) atoms connected by l_m are renormalized (removed), the remaining atoms (blue and green) form a new pair with an effective distance that happens to be l. This increases the probability of finding a pair with effective distance l in the chain. Thus the probability change caused by this process needs to be added to $P(l, l_m)$, which gives the third term in the larger square bracket on the RHS of Eq. (C1). Finally, one is reminded that $P(l, l_m)$ is a probability distribution and needs to fulfill the normalization condition. Note that every time a pair with effective distance l_m is eliminated from the chain, the total number of pairs remaining in the chain is decreased by 2, therefore the new probability distribution needs to be renormalized by dividing the fraction of all the remaining pairs in the chain, which corresponds to the inverse factor on the RHS of Eq. (C1).

$$P(l, l_m + \Delta) = [1 - 2\Delta P(l_m, l_m)]^{-1}\Bigg[P(l, l_m) - 2\Delta P(l_m, l_m)P(l, l_m)\int_{l_m}^{\infty} dx P(x, l_m) + \Delta P(l_m, l_m)\int_{l_m}^{\infty} dx\, dy\, P(x, l_m)P(y, l_m)\,\delta(x + y + l_m - d_{\text{eff}} - l)\Bigg]. \tag{C1}$$

By performing the change of variables $\lambda = l/l_m - 1$ and $Q(\lambda, l_m) = l_m P(l, l_m)$, after some algebra, one reaches Eq. (2) in the main text.

2. Initial condition for the flow equation

We assume that atoms are randomly distributed among the trapping sites near the PCW, with probability $P = N/N_{\text{site}}$, under the conditions $N, N_{\text{site}} \to \infty$, where N and N_{site} are the total number of atoms and lattice sites, respectively. Then, starting from any occupied site in the spin chain, the probability of finding the next atom at the nth next site away is

$$\mathcal{P}(l = na, l_m = a) = P(1 - P)^{n-1}. \tag{C2}$$

This is equivalent to the probability of finding two atoms positioned $l = na$ apart, when the smallest distance between two atoms in the whole system is $l_m = a$, with a being the lattice constant. We note the normalization condition that Eq. (C2) fulfills:

$$\sum_{n=1}^{+\infty} P(1 - P)^{n-1} = 1. \tag{C3}$$

To line up the solution of the flow equation at the beginning as much as possible with this discrete distribution, we may approximate it by a continuous distribution:

$$\mathcal{P} \to P(1 - P)^{l/l_m - 1}\frac{dl}{l_m} \equiv P(l, l_m)\, dl, \tag{C4}$$

where l is a continuous variable and $P(l, l_m)$ is a *probability density*. Enforcing normalization condition $\int_{l_m}^{+\infty} P(l, l_m)\, dl = 1$ we obtain the initial condition for the flow equation Eq. (2) in the main text:

$$Q(\lambda, l_m = a) = -\ln(1 - P)(1 - P)^{\lambda}. \tag{C5}$$

3. Fraction of unpaired atoms

With the solution of $P(l, l_m)$ we can estimate the fraction of unpaired atoms when the shortest effective distance in the system is l_m. To do this, we first define the number of unpaired atoms in the system at this stage as $N(l_m)$, and note $N(l_m = a) = N$. Then the number of couplings left in the system at this stage is $N(l_m) - 1 \approx N(l_m)$. The number of couplings that are to be removed from the system in the next step is then

$$dN(l_m) = -2P(l_m, l_m)\, dl_m\, N(l_m). \tag{C6}$$

Changing l_m to a dummy variable l'_m and integrating from a to l_m, and noting that $N(l_m = a) = N$, one obtains

$$N(l_m) = N \exp\left(-2\int_a^{l_m} P(l'_m, l'_m)\, dl'_m\right). \tag{C7}$$

4. Derivation of the joint flow equation

Similar as for $P(l, l_m)$, a flow equation for the nested probability distribution $P(n_l, l, l_m)$ can be constructed as

$$\begin{aligned} &P(n_l, l, l_m + \Delta)\left(1 - 2\Delta\sum_{n_{l_m}=0}^{+\infty} P(n_l, l_m, l_m)\right) \\ &= P(n_l, l, l_m) - 2\Delta P(n_l, l, l_m)\sum_{n_{l_m}=0}^{+\infty} P(n_l, l_m, l_m) \\ &\quad + \Delta \cdot \sum_{n_{l_m}, n_x, n_y = 0}^{+\infty} \delta_{n_x + n_{l_m} + n_y + 1, n_l} P(n_{l_m}, l_m, l_m) \\ &\quad \times \int_{l_m}^{+\infty} dx\, dy\, P(n_x, x, l_m)P(n_y, y, l_m) \\ &\quad \times \delta[x + y + l_m - d_{\text{eff}}(l_m) - l], \end{aligned} \tag{C8}$$

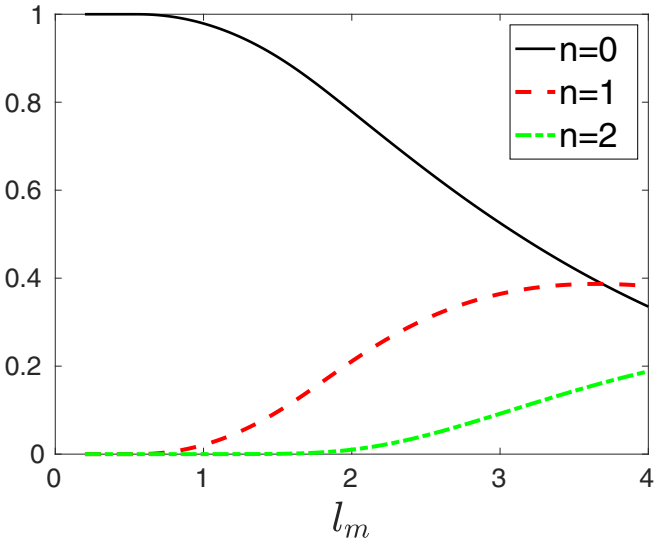

FIG. 6. Fractions of un-nested ($n = 0$) and nested ($n = 1, 2$) pairs at pair length l_m for 12% filling fraction.

where the terms have similar meanings as those in Eq. (C1). We note n_l can take any non-negative integer values $n_l = 0, 1, 2, \ldots$ and initially when $l_m = a$, $n_l = 0$ for all l.

Again, introducing the substitutions $\lambda = l/l_m - 1$ and $P(n_l, l, l_m)dl = Q(n_\lambda, \lambda, l_m)d\lambda$, after some algebra, one obtains

$$l_m \frac{\partial Q}{\partial l_m} - (1+\lambda)\frac{\partial Q}{\partial \lambda} = Q + \sum_{n_0=0}^{n_\lambda - 1} Q(n_0, 0, l_m) \sum_{n_x=0}^{n_\lambda - 1 - n_0} \int_0^{\lambda + g(l_m)} d\lambda_x Q(n_x, \lambda_x, l_m) Q(n_\lambda - 1 - n_0 - n_x, \lambda + g(l_m) - \lambda_x, l_m). \quad \text{(C9)}$$

APPENDIX D: FRACTIONS OF NESTED PAIRS AT THE END OF TIME EVOLUTION

At the optimal slew rate mentioned in the main text, the weakest interaction strength of a pair preserved is $\tilde{J}_{ij} \approx 0.12 J_0$, which corresponds to the longest pair length of $l_{\max} \approx 2.1$ (in units of L). In Fig. 6, we plot the fractions of un-nested and nested pairs vs pair lengths for 12% filling fraction. One can see that in the range $l_m \leqslant 2.1$, the fraction of nested pairs ($n > 0$) has become significant. Greater fractions of nested pairs can be obtained by having longer pairs preserved, at the expense of lower overall fidelity by going slower in the adiabatic evolution.

[1] P. Lodahl, S. Mahmoodian, and S. Stobbe, Rev. Mod. Phys. **87**, 347 (2015).
[2] D. E. Chang, J. S. Douglas, A. Gonzalez-Tudela, C.-L. Hung, and H. J. Kimble, Rev. Mod. Phys. **90**, 031002 (2018).
[3] E. Vetsch, D. Reitz, G. Sague, R. Schmidt, S. T. Dawkins, and A. Rauschenbeutel, Phys. Rev. Lett. **104**, 203603 (2010).
[4] A. Goban, K. S. Choi, D. J. Alton, D. Ding, C. Lacroute, M. Pototschnig, T. Thiele, N. P. Stern, and H. J. Kimble, Phys. Rev. Lett. **109**, 033603 (2012).
[5] R. Mitsch, C. Sayrin, B. Albrecht, P. Schneeweiss, and A. Rauschenbeutel, Nat. Commun. **5**, 5713 (2014).
[6] H. L. Sorensen, J. B. Beguin, K. W. Kluge, I. Iakoupov, A. S. Sorensen, J. H. Muller, E. S. Polzik, and J. Appel, Phys. Rev. Lett. **117**, 133604 (2016).
[7] N. V. Corzo, B. Gouraud, A. Chandra, A. Goban, A. S. Sheremet, D. V. Kupriyanov, and J. Laurat, Phys. Rev. Lett. **117**, 133603 (2016).
[8] N. V. Corzo, J. Raskop, A. Chandra, A. S. Sheremet, B. Gouraud, and J. Laurat, Nature **566**, 359 (2019).
[9] S. Kato, N. Nemet, K. Senga, S. Mizukami, X. Huang, S. Parkins, and T. Aoki, Nat. Commun. **10**, 1160 (2019).
[10] T. Lund-Hansen, S. Stobbe, B. Julsgaard, H. Thyrrestrup, T. Sunner, M. Kamp, A. Forchel, and P. Lodahl, Phys. Rev. Lett. **101**, 113903 (2008).
[11] A. Javadi, I. Sollner, M. Arcari, S. L. Hansen, L. Midolo, S. Mahmoodian, G. Kirsanske, T. Pregnolato, E. H. Lee, J. D. Song, and P. Lodahl, Nat. Commun. **6**, 8655 (2015).
[12] A. Goban, C. L. Hung, S. P. Yu, J. D. Hood, J. A. Muniz, J. H. Lee, M. J. Martin, A. C. McClung, K. S. Choi, D. E. Chang, O. Painter, and H. J. Kimble, Nat. Commun. **5**, 3808 (2014).
[13] J. D. Hood, A. Goban, A. Asenjo-Garcia, M. Lu, S.-P. Yu, D. E. Chang, and H. J. Kimble, Proc. Nat. Acad. Sci. **113**, 10507 (2016).
[14] M. E. Kim, T.-H. Chang, B. M. Fields, C.-A. Chen, and C.-L. Hung, Nat. Commun. **10**, 1647 (2019).
[15] H. J. Kimble, Nature (London) **453**, 1023 (2008).
[16] D. O'Shea, C. Junge, J. Volz, and A. Rauschenbeutel, Phys. Rev. Lett. **111**, 193601 (2013).
[17] T. G. Tiecke, J. D. Thompson, N. P. de Leon, L. R. Liu, V. Vuletic, and M. D. Lukin, Nature (London) **508**, 241 (2014).
[18] I. Shomroni, S. Rosenblum, Y. Lovsky, O. Bechler, G. Guendelman, and B. Dayan, Science **345**, 903 (2014).
[19] M. Scheucher, A. Hilico, E. Will, J. Volz, and A. Rauschenbeutel, Science **354**, 1577 (2016).
[20] J. S. Douglas, H. Habibian, C.-L. Hung, A. V. Gorshkov, H. J. Kimble, and D. E. Chang, Nat. Phot. **9**, 326 (2015).
[21] A. Gonzalez-Tudela, C.-L. Hung, D. E. Chang, J. I. Cirac, and H. J. Kimble, Nat. Phot. **9**, 320 (2015).
[22] C.-L. Hung, A. Gonzalez-Tudela, J. I. Cirac, and H. J. Kimble, Proc. Nat. Acad. Sci. **113**, E4946 (2016).
[23] M. T. Manzoni, L. Mathey, and D. E. Chang, Nat. Commun. **8**, 14696 (2017).
[24] A. S. Prasad, J. Hinney, S. Mahmoodian, K. Hammerer, S. Rind, P. Schneeweiss, A. S. Sorensen, J. Volz, and A. Rauschenbeutel, Nat. Phot. **14**, 719 (2020).
[25] S. Mahmoodian, G. Calajó, D. E. Chang, K. Hammerer, and A. S. Sørensen, Phys. Rev. X **10**, 031011 (2020).
[26] G. Kurizki, Phys. Rev. A **42**, 2915 (1990).
[27] S. John and T. Quang, Phys. Rev. Lett. **76**, 1320 (1996).

[28] S. Bay, P. Lambropoulos, and K. Molmer, Phys. Rev. A **55**, 1485 (1997).
[29] E. Shahmoon and G. Kurizki, Phys. Rev. A **87**, 033831 (2013).
[30] F. Liu, R. Lundgren, P. Titum, G. Pagano, J. Zhang, C. Monroe, and A. V. Gorshkov, Phys. Rev. Lett. **122**, 150601 (2019).
[31] J. S. Douglas, T. Caneva, and D. E. Chang, Phys. Rev. X **6**, 031017 (2016).
[32] E. Shahmoon, P. Grisins, H. P. Stimming, I. Mazets, and G. Kurizki, Optica **3**, 725 (2016).
[33] C. Dasgupta and S.-k. Ma, Phys. Rev. B **22**, 1305 (1980).
[34] D. S. Fisher, Phys. Rev. B **50**, 3799 (1994).
[35] U. Schollwock, Ann. Phys. **326**, 96 (2011).
[36] A. Polkovnikov, K. Sengupta, A. Silva, and M. Vengalattore, Rev. Mod. Phys. **83**, 863 (2011).
[37] L. D. Landau, Phys. Z. Sowjetunion **2**, 46 (1932); see also, *Collected Papers of L. D. Landau*, edited by D. ter Haar (Pergamon, Oxford, 1965).
[38] L. D. Landau and E. M. Lifshitz, *Quantum Mechanics: Non-relativisitic Theory*, 3rd ed. (Pergamon, New York, 1977).
[39] C. Zener, Proc. R. Soc. A **137**, 696 (1932).
[40] M. Endres, H. Bernien, A. Keesling, H. Levine, E. R. Anschuetz, A. Krajenbrink, C. Senko, V. Vuletic, M. Greiner, and M. D. Lukin, Science **354**, 1024 (2016).
[41] D. Barredo, S. d. Leseleuc, V. Lienhard, T. Lahaye, and A. Browaeys, Science **354**, 1021 (2016).
[42] W. Lee, H. Kim, and J. Ahn, Phys. Rev. A **95**, 053424 (2017).
[43] D. Barredo, V. Lienhard, S. d. Leseleuc, T. Lahaye, and A. Browaeys, Nature (London) **561**, 79 (2018).
[44] M. O. Brown, T. Thiele, C. Kiehl, T.-W. Hsu, and C. A. Regal, Phys. Rev. X **9**, 011057 (2019).
[45] P. Samutpraphoot, T. Dordevic, P. L. Ocola, H. Bernien, C. Senko, V. Vuletic, and M. D. Lukin, Phys. Rev. Lett. **124**, 063602 (2020).
[46] X. Luan, J.-B. Beguin, A. P. Burgers, Z. Qin, S.-P. Yu, and H. J. Kimble, Adv. Quantum Technol. **3**, 2000008 (2020).
[47] E. Kim, X. Zhang, V. S. Ferreira, J. Banker, J. K. Iverson, A. Sipahigil, M. Bello, A. Gonzalez-Tudela, M. Mirhosseini, and O. Painter, Phys. Rev. X **11**, 011015 (2021).
[48] K. Hammerer, A. S. Sorensen, and E. S. Polzik, Rev. Mod. Phys. **82**, 1041 (2010).
[49] Z. Chen, J. G. Bohnet, J. M. Weiner, K. C. Cox, and J. K. Thompson, Phys. Rev. A **89**, 043837 (2014).
[50] N. Behbood, F. M. Ciurana, G. Colangelo, M. Napolitano, G. Toth, R. J. Sewell, and M. W. Mitchell, Phys. Rev. Lett. **113**, 093601 (2014).
[51] D. A. Abanin, E. Altman, I. Bloch, and M. Serbyn, Rev. Mod. Phys. **91**, 021001 (2019).
[52] N. Fayard, L. Henriet, A. Asenjo-Garcia, and D. Chang, arXiv:2101.1645v2.
[53] H. P. Breuer and F. Petruccione, *The Theory of Open Quantum Systems* (Oxford University Press, Oxford, 2002).
[54] S. Bravyi, D. P. DiVincenzo, and D. Loss, Ann. Phys. **326**, 2793 (2011).